Sychterz, A.C. and Smith, I.F.C. "Using dynamic measurements to detect and locate ruptured cables on a tensegrity structure", Eng. Structures, 173, 2018, pp 631-642 doi:10.1016/j.engstruct.2018.06.083

Using dynamic measurements to detect and locate ruptured cables on a tensegrity structure

Ann C. Sychterz[a,*], Ian F. C. Smith[a]

[a] *Applied Computing and Mechanics Laboratory (IMAC), School of Architecture, Civil and Environmental Engineering (ENAC), Swiss Federal Institute of Technology Lausanne (EPFL), CH-1015 Lausanne, Switzerland*

Abstract

Tensegrity structures are cable-strut systems held in equilibrium due to self-stress. There is potential for damage tolerance when they are kinematically redundant. In this paper, detection and location of a ruptured cable in a deployable tensegrity footbridge are studied through monitoring changes in dynamic behavior. Position values and axial load values of elements are measured before, during, and after a cable breakage. Free and forced-vibration-induced dynamic behavior of the tensegrity structure are characterized in the state of deployment (one half of the structure) and in-service (full structure). Examination of ambient vibrations for the half structure and forced vibrations for the full structure successfully led to detection of ruptured cables. Exclusion of possible damage cases for location using measurements effectively reduces the number of candidate cases when using nodal displacement measurements. Correlation methods using strain measurements are also successful to locate a ruptured cable. These methods reveal the potential for self-diagnosis of complex sensed structures.

Keywords: Detection, location, tensegrity structure, dynamic response, cable rupture

1. Introduction

Civil-engineering structures are designed to resist loading that is expected throughout the lifetime of the structure. Through large deformation capacity and connectivity redundancy,

*Corresponding author. Address: EPFL ENAC IIC IMAC, Station 18, CH-1015 Lausanne, Switzerland. Phone number: +41 21 693 2498

Email address: ann.sychterz@epfl.ch (Ann C. Sychterz)

they also have to provide warning prior to collapse.

Deployable structures have been studied for decades in civil engineering (Gantes et al., 1989; Pellegrino, 2001; Akgün et al., 2011). Tensegrity structures are closely coupled systems composed of struts and cables held in equilibrium by self-stress (Skelton et al., 2001; Snelson, 2012; Motro, 2011; Pellegrino and Calladine, 1986). When redundancy is present in these structures, a cable rupture might cause only a serviceability-state violation rather than an ultimate limit-state violation.

Measurement of static structural response led to identification of damage location (self-diagnosis) in a tensegrity structure by Adam and Smith (2007a). Slope measurements of the laboratory structure and simulations of possible scenarios were compared. Perturbations using small actuator movements were carried out to classify the strength of possible scenarios. To date, this method for detection has been limited to small actuation movements.

Damage identification using vibration characteristics was reviewed by Doebling et al. (1996) who summarized data-interpretation methods. Friswell (2007) gave a summary of inverse methods for damage identification. Ashwear and Eriksson (2014) introduced a known perturbation to measure the dynamic response of actively-controlled structures. Damage resulted in a response that was not expected for an undamaged structure. Ashwear and Eriksson (2017) have also made vibration-based health monitoring simulation studies of a 2D tensegrity structure. No studies included work on damage detection using vibration characteristics for deployable tensegrity structures.

A major challenge associated with natural frequency-based detection is that changes due to ruptured cables can be smaller than the effect of changes in environmental and operational conditions (Fan and Qiao, 2010). Yin et al. (2017) used a Bayesian approach with model reduction for damage detection using vibration measurements of a two-storey frame. The review by Fan and Qiao (2010) did not identity successful methods for damage detection in complex structures.

In tensegrity structures, characterizing damage is straightforward since structural elements are discrete elements that are subjected mainly to axial force. Khellaf and Kebiche (2013) used a Lagrangian formulation to perform a static analysis of the effect of slackened

and yielded cables. Bhalla et al. (2013) investigated damage assessment in a four module tensegrity grid. Shekastehband et al. (2011) have studied sensitivity of tensegrity structures to member loss and dynamic propagation of rupture (Shekastehband and Abedi, 2014). Damage detection was based on modal analysis. Although their methodology has been able to locate damaged elements, the structure had a relatively simple geometry that did not undergo large displacements.

Kahla and Kebiche (2000) studied the response of a five-module tensegrity structure. The investigation included non-linear elasto-plastic analysis and partial damage such as cable yielding and the dynamic response was studied. Following this study, Kahla and Moussa (2002) analyzed the effect of a cable rupture on tensegrity systems through nonlinear dynamic simulation (Sultan et al., 2002). Neither cable yielding nor strut buckling was included in the study. Although damage tolerance of a tensegrity system in case of sudden cable breakage was demonstrated, no generalization was proposed.

Effects of active perturbations on the slope of the structure and those for the remaining candidates were then compared by Adam and Smith (2007b). The candidate scenario for which the difference was weakest was accepted along with candidates within an error band which was a function of the precision of the active-control system. These were classified as potentially correct solutions for self-diagnosis (Adam and Smith, 2007a). Although the candidate nearest to the behavior of the physical structure was not always the one located at the same node as the load applied, the exact location of the load was not always necessary to find the best possible slope compensation. Self-diagnosis was thus shown to direct active control for intelligent structural behavior during situations of partially defined loading events and damage. This structure was not deployable.

This paper describes strategies for detection and location of ruptured cables in a near-full-scale deployable tensegrity footbridge using displacement and strain measurements. Both the half structure (during deployment) and full structure (in-service) tensegrity structure cases are included. A frequency analysis method (see Section 2.1), a population-exclusion method (see Section 2.2), and a principal component analysis method (see Section 2.3) are compared for detection and location of ruptured cables. In Section 5.1.1, dynamic behavior

is simulated using a finite element model and compared with measurements taken from the tensegrity structure. Free-vibration and forced-vibration tests have been implemented on the structure to compare structural behavior with and without in-service loading (see Section 5.1.2). All tests have been completed for the structure in healthy and damaged states, where a cable has been ruptured. Natural frequencies and nodal positions of the structure were used to detect the occurrence of damage. Location of damage utilized both dynamic and static behavior of the structure (see Section 5.2.1). Strain and displacement measurements were also used for location of ruptured cables (see Section 5.2.3).

The original contribution of this paper is an evaluation of the ability of several methods to detect and locate damage in a near-full-scale deployable tensegrity structure. All methods have potential to be applied to other active structures.

2. Background

This section provides detail related to data analysis techniques that have been used to support the methodologies proposed in this paper.

2.1. Signal processing methods: Second order blind identification (SOBI)

Statistical signal processing tools have been used extract properties of the structure (called modal extraction). The process of modal extraction applies elementary signal processing concepts to the linear equation of motion, specifically:

$$\begin{aligned} \mathbf{M}\ddot{\mathbf{x}}(t) + \mathbf{C}\dot{\mathbf{x}}(t) + \mathbf{K}\mathbf{x}(t) &= \mathbf{F}(t) \\ \ddot{\mathbf{x}}(t) + 2\omega_n\zeta\dot{\mathbf{x}}(t) + \omega_n^2\mathbf{x}(t) &= \mathbf{F}(t) \end{aligned} \tag{1}$$

where $\mathbf{x}(t)$ is the time-domain signal, ζ is the damping ratio, ω_n is the natural frequency, $\mathbf{F}(t)$ is the applied excitation, $\mathbf{M}$ is the mass matrix of the system, $\mathbf{C}$ is the damping matrix of the system, and $\mathbf{K}$ is the stiffness matrix of the system. The particular method used in this study to separate the source signal has been called stochastic subspace identification (SSI) (Overschee and Moor, 1996). Collected acceleration data has been used in the estimation of the state-space solution of the second-order differential equation, Equation 1. Gaussian

white noise has been superimposed onto the state-space model in the stochastic analysis [2]. The state-space model has been defined as:

$$\begin{aligned} \dot{\mathbf{z}}(t) &= \mathbf{A}(t)\mathbf{z}(t) + \mathbf{B}(t)\mathbf{u}(t) \\ \mathbf{y}(t) &= \mathbf{C}(t)\mathbf{z}(t) + \mathbf{D}(t)\mathbf{u}(t) \end{aligned} \tag{2}$$

where $\mathbf{z}$ is the state-vector, $\mathbf{y}$ is the output vector, $\mathbf{A}$ is the system matrix, $\mathbf{C}$ is the output matrix. Although $\mathbf{B}$ and $\mathbf{D}$ are the input and feedthrough matrices respectively with $\mathbf{u}$ as the input vector, since zero-mean Gaussian noise has been being added to the system, the second terms of each of these equations is simplified to a set of Gaussian noise vectors.

The eigenvalues λ, and eigenvectors Θ, were determined from the decomposition of matrix A (Poncelet et al., 2010). Given an ordinate number of greater than 2 times the size of matrix A, it is possible to complete the eigenvalue problem. The eigenvalues were used to solve for the natural frequencies of the system. The specific method of applying SSI for this study was a Numerical algorithm for Subspace State Space System IDentification (N4SID).

The following three steps were used to initialize SOBI: whitening, orthogonalization, and unitary transformation. Whitening is a linear transformation where the covariance matrix at zero time-lag is first diagonalized using singular value decomposition. Orthogonalization was next applied to diagonalize the covariance matrix at a time-lag. The task then involves unitary diagonalization of the correlation matrix at one or several non-zero time lags. The determination of the unitary matrix was carried out using a numerical procedure, commonly known as joint approximate diagonalization Belouchrani and Abed-meraim (1997).

Once A was estimated from Equation 2, the sources was estimated using the pseudo-inverse of Equation 1. Sources identified natural frequencies of the structure using a model-free method. To determine the location of the damaged element, a model-based method was required to compare measurements with simulations, see Section 5.

2.2. Error-domain model falsification (EDMF)

Rather than performing optimization to find one result, exclusion of possible scenarios, as discussed by Popper (1959), allows for more flexibility in uncertain conditions. His

reasoning was that a hypothesis cannot be fully validated using measurement. Since then, many researchers have also discussed the benefits of exclusion of scenarios to accommodate bias while interpreting observations (Beck, 1987; Popper, 1959; Beven and Binley, 1992; Tarantola, 2006). The subsequent difficulty has been to establish the generalized likelihood uncertainty estimation (GLUE) criterion that identify models (Beven et al., 2008; Zhang and Li, 2015; Sun et al., 2014; Blasone et al., 2008).

A methodology has been proposed called error-domain model falsification (EDMF), that compared prediction with measurements while taking many sources of uncertainty, including model bias, into account (Smith, 2016). Threshold bounds are distinguished between possible scenarios that explain measurements (candidate scenarios) and those that do not (excluded scenarios) (Figure 1). Possible scenarios were generated through sampling combinations of parameter values in a model class.

The probability density function shown in Figure 1. Latin Hypercube Sampling (LHS) (McKay et al., 1979) determined combined uncertainties for the Monte-Carlo analysis (Smith, 2016). Threshold values were defined in order to ensure a reliability of identification. If target probability of identification is $x\%$, there is $(100 - x)\%$ probability to exclude the correct scenario. When more than one measurement was used, threshold values are adjusted by the Šidák correction (Sidak, 1967) to ensure that the target reliability of identification over all comparisons has remained constant. A typical target reliability of identification is 95%. Differences between measurements and model predictions at measurement locations are calculated. When the difference is outside of the threshold values, a model is excluded (rejected).

2.2.1. Applications of scenario exclusion using EDMF

The EDMF methodology has been used for diagnosis tasks in structural engineering (Smith, 2016). Adam and Smith (2007a) also used an exclusion procedure with static measurements to detect and locate damaged in an active structure with small shape changes. Although candidates having damage locations nearest to the behavior of the physical structure have not always been located at the true location of damage, exact location of loading

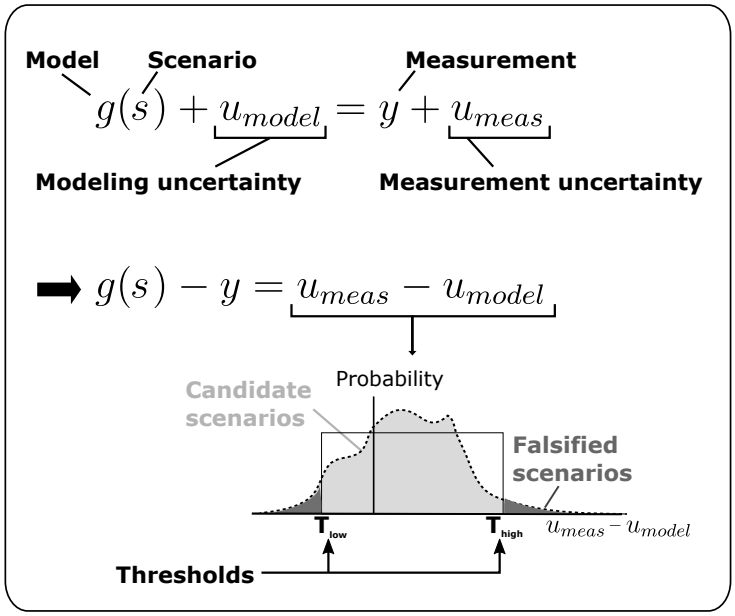

Figure 1: Error domain model falsification (EDMF). The unknown form of the probability density function is approximated by a uniform probability distribution shown by the rectangle.

was not always necessary to find the best possible actuation movements for self-repair. These two observations led to the conclusion that sets of good solutions were sufficient.

Using EDMF for damage location in this structure has required iterations of a static analysis method called dynamic relaxation (DR) using pseudo-dynamic vector-based system and kinematic damping. First used in structural engineering by Day (1965) and Otter (1965), the method was improved by Bel Hadj Ali et al. (2011) in order to accommodate continuous cables over nodes and friction (Sychterz and Smith, 2017).

Previous work on damage detection using static methods and model exclusion algorithms for this tensegrity structure has been carried out by Veuve (2015). Discontinuous cables have been uninstalled from the structure to simulate the loss of integrity in a cable. Additional loading was applied on the structure in its healthy and damaged states in order to detect damage. EDMF was able to successfully falsify only 50% of the damage scenarios. This work has been extended in the remainder of this paper to simulate cable rupture more realistically.

Table 1: Summary of goals for damage detection and location and the methodology involved

Goal	Methodology	Section
Detection of damaged element (static)	Second-order blind identification (SOBI)	5.1.1
Location of candidate damaged element	Error-domain model falsification (EDMF)	5.2.1
Location of elements most influenced by damage	Moving-window principal component analysis (MWPCA)	5.2.3

2.3. Damage location using moving-window principal component analysis (MWPCA)

Several model-free methodologies for continuously-monitored structures were discussed by Posenato et al. (2008) and were applied to damage detection. Amongst other methods, anomaly detection in continuously-monitored structures by Laory et al. (2013) utilized principal component analysis (PCA).

Principal component analysis helped identify uncorrelated components through an orthogonal transformation (Pearson, 1901). PCA used all measurements and searched for changes in eigenvectors between sets of measurements. Damage was detected when change in an eigenvector was greater than the threshold of statistical significance which is taken to be six times the standard deviation (6σ) of eigenvector variance. Moving window PCA (MWPCA) is useful for detecting a peak shift in the eigenvalues and is applied over a set of time intervals (see Section 2.3). The implementation of MWPCA for damage location for damage detection for structures undergoing large shape changes has not yet been studied. Table 1 shows the goals for damage detection and location and the methodology involved.

3. Deployable active tensegrity structure

This section provides a description of the laboratory structure. The topology shown in Figure 2 is called a hollow-rope and it has been proposed by Motro et al. (2006) for a pedestrian footbridge. At full-scale, the center opening of the 16 m-long bridge is large enough for pedestrian traffic. This geometrically nonlinear structure (Kebiche et al., 1999) has been used for the experiment, has taken advantage of a closely-coupled multi-element configuration to deploy along several degrees of freedom.

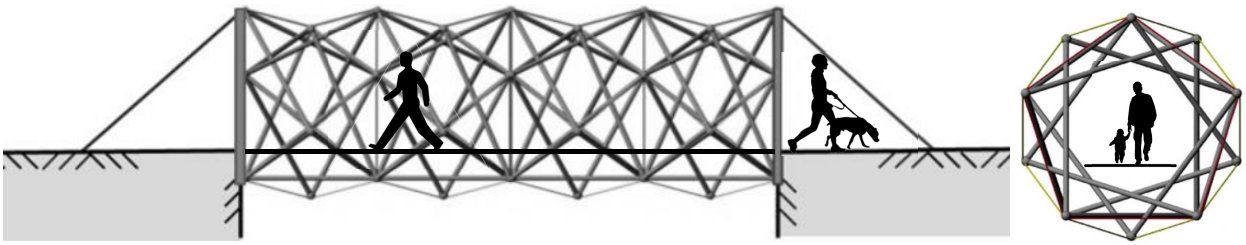

Figure 2: Side (left) and front (right) views of tensegrity footbridge schematic.

Figure 3 shows a 1/4-scale of the proposed tensegrity structure when deployed and connected at mid-span. The tensegrity structure has been modeled in two configurations; the full connected structure under pre-stress and the half structure prior to mid-span connection. Position sensors (square) and strain gauges (circle) are shown. The numbering of position sensors is arbitrary with the exception that the first three sensors are installed at end-nodes of the structure. Strain gauges are noted with number of the element to which they are installed.

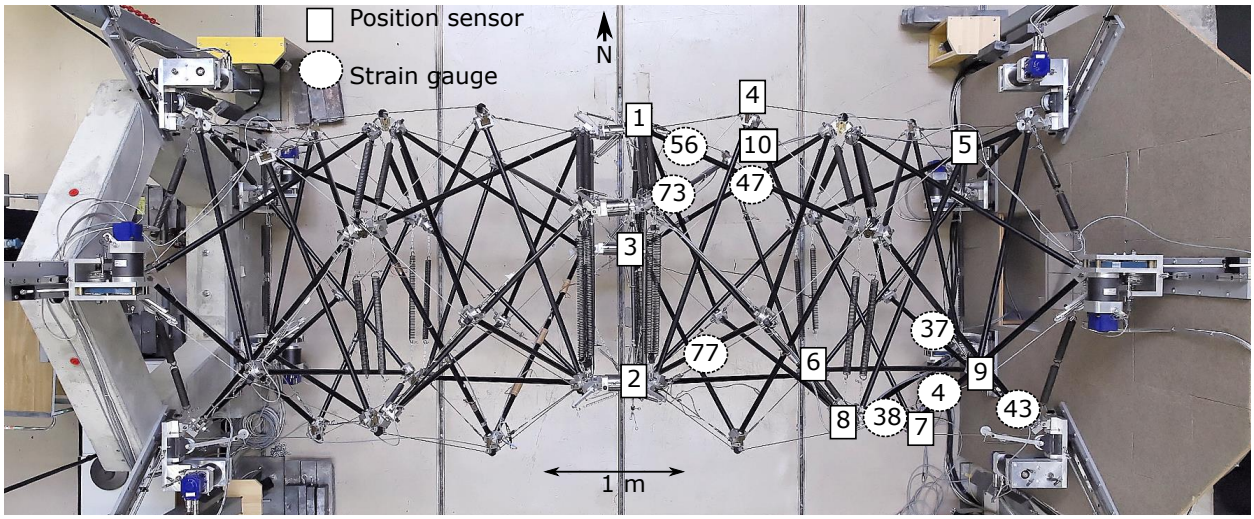

Figure 3: Top view of deployed and connected deployable tensegrity footbridge with continuous cables. Position sensors (square) and strain gauges (circle) are shown. [Credit: IMAC, EPFL]

The near-full-scale steel tensegrity structure is 4 [m] in length, 1.5 [m] in height, and 1.5 [m] in width. It has been constructed in two halves that deploy and connect at mid-span.

Each half is composed of two pentagonal ring modules with a total of fifteen low-stiffness elements (springs), twenty discontinuous cables, thirty struts, and five continuous active cables (Bel Hadj Ali et al., 2010). Struts are tubes with a diameter of 28 [mm], thickness of 1.5 [mm] and a length of 1.35 [m]. Cables are seven braided-steel-strand, 3 [mm] in diameter. Springs near the supports of the structure have a stiffness value of 2 [kN/m] and 2.9 [kN/m] in the rest of the structure (Rhode-Barbarigos et al., 2012; Veuve et al., 2015). These springs facilitate deployment by storing energy when the diameter increases during folding. Each half of the structure weighs approximately 100 [kg] and connecting node pairs are joined sequentially due to self-weight deflection of the structure. Two half-tensegrity structures connect and form a full-tensegrity structure.

The tensegrity structure is composed of four identical modules, two modules per half. Within each module, there is a pentagonal ring with five nodes on each end of the module as well as an intermediate pentagonal ring. A cable segment is defined as a length of cable between two adjacent nodes. Discontinuous cables connect nodes over one segment. Along each continuous cable path, there are four segments for each half of the tensegrity structure. Actuation of the structure originates from the motor winding and unwinding of an active (continuous) cable onto a drum at the supports. The structure is kinematically indeterminate with six states of self-stress, an arrangement of internal forces in a multi-element system in equilibrium Rhode-Barbarigos et al. (2010).

4. Testing of cable rupture in the tensegrity structure

One discontinuous cable (refer to description of the structure) from each section of the half structure with the largest tensile loads were been selected for the rupture event. Since the half structure was a cantilever, all cable segments selected for testing were located on the top half as shown in Figure 4.

Dynamic simulations were carried out using a software called SOFiSTiK (SOFiSTiK, 2017). Benefits included the possibility to simulate continuous cables along the length of each half structure and cables with sag. Simulations involved the assumption that nodes were without eccentricity and modeling sliding-friction with this software was not possible.

Struts in this model were beam elements, taking bending moments into account. Comparison of simulations with measurements was useful for understanding behavior (Dubé et al., 2008).

A rupture event was most likely to occur in highly-stressed cables. Since continuous-cable stress values were more uniform in the folded state than in the deployed state and discontinuous cables carried little to no tension in the folded state, cable rupture in the folded state was not tested.

In the connected and pre-stressed state, cables carried the highest tension at the top near the supports and on the bottom of the structure at mid-span. Since it was likely that a cable either broke during deployment or when the two-halves of the bridge were connected, both these states were simulated. A rupture event during deployment was a concern for completing deployment while a rupture event during in-service conditions could lead to an exceedance of a critical limit state.

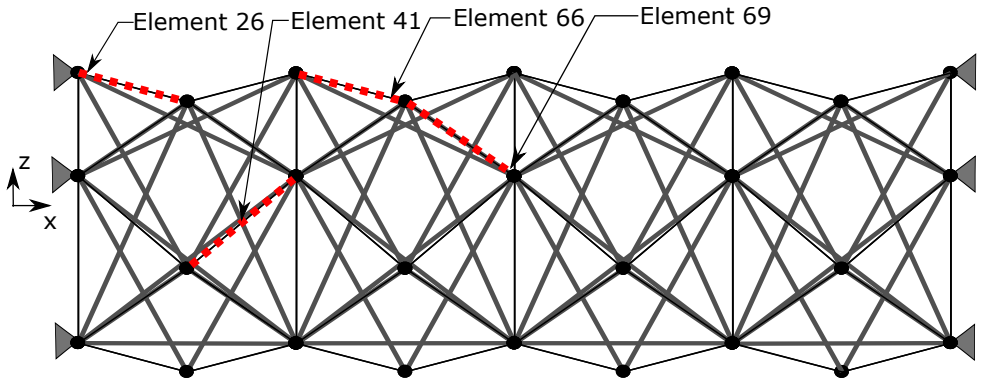

Figure 4: Elevation sketch of deployed and connected structure. Cables involved in the rupture study (Elements 26, 41, 66 and 69) are shown.

An electromagnet attached to connector plates the end of a discontinuous cable is shown in Figure 5. The electromagnet was activated to resist a tensile load up to 1 kN. When discharged, the electromagnet released instantly, simulating a cable rupture.

The measurement duration included 10 seconds pre-rupture and 20 seconds post-rupture. Nodal positions were measured using an optical tracking system, OptiTrack with eight Prime 13 cameras (see Figure 6). These cameras were installed on the four corners of each support of the structure. Strain gauges, HBM type LY41 for cables and type LY11 for struts, measured

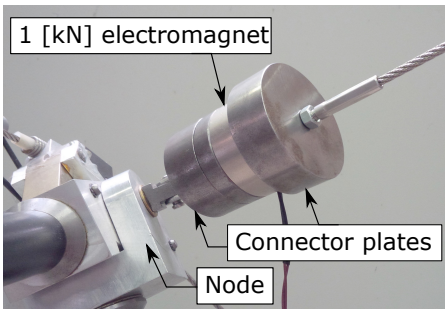

Figure 5: Discontinuous cable fitted with an electromagnet with a tensile force of 1 [kN] when activated. It is able to simulate repeated rupture events.

axial loads in elements. Transfer sensitivity of the strain gauges on the cables and struts were 0.1 % and 0.3 % respectively. Load cells, HBM U9C 10 [kN] 1]mV/V] with 1 % sensitivity, were installed on the continuous cables at mid-span.

A sensitivity analysis was conducted to determine the number of sensors required for successful use of measurements in the scenario-exclusion method (see Section 2.2). This algorithm involved measurements of nodal positions using motion tracking rather than strain gauge measurements due to signal clarity. Despite correctly estimated uncertainties, too few sensor locations resulted in poor measurements to compare with simulations and thus ineffective for the EDMF method. To falsify scenarios with a low risk of redundant sensors, six sensor positions were required for the half-tensegrity-structure and eight for the full-tensegrity structure. For the full-tensegrity structure, eight sensor positions were required for a low risk of redundant sensors. Position sensors were subject to occlusion from other sensors or the structure, thus ten position sensors were installed for testing.

Sensor placement was an important aspect when studying the response of a structure. Strain gauges were distributed throughout the structure. Groups of spherical markers, called rigid bodies, shown in Figure 6, were installed on nodes that had the highest response energy due to a rupture of any cable in the structure. This energy was a measure of tension force in elements adjacent to a node multiplied by displacement of that node following rupture. Since the cables to be damaged as part of the rupture event were chosen based on the highest forces in discontinuous cables, the rigid bodies were often installed at nodes of the damaged cables.

Tests were conducted at least ten times per cable for both the half and full-tensegrity structure. All data was acquired at 165 [Hz] while avoiding lag in data acquisition for the combined optical tracking system, the strain gauges and load cells.

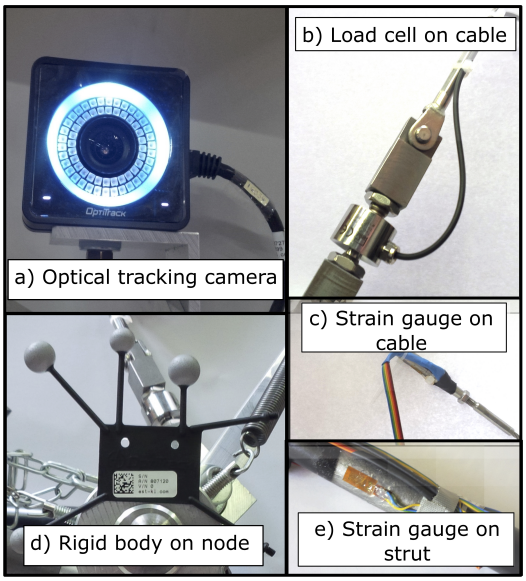

Figure 6: Optical tracking camera (one of eight) (a), load cells on continuous cables (b), strain gauges on cables (c), optical tracking rigid body on nodes (d), and strain gauges on struts (e).

5. Methodologies and Results

Nodal position data from the start of the rupture event until the end of the test have been processed using the second-order blind identification (SOBI) (see Section 2.1) method to separate the natural frequencies of the system. Natural frequencies have been identified for the half-tensegrity structure using ambient vibrations and for the full-tensegrity structure using forced-vibrations such that source separation was possible. Analysis of damage location using moving window principal component analysis (MWPCA) for strain measurements utilized a variation limit of 6σ and error-domain model falsification (EDMF) for position measurements utilized a variation limit of 2σ. The wider variation limit for strain measurements was possible since MWPCA compares variations in values of eigenvectors. Small values of σ were often below measurement resolution. Position measurements were used for EDMF

Table 2: Average measurements of natural frequencies from ten tests on the half structure for rupture of Elements 26, 41, 66, and 69 including variation of 2 standard deviations, approximately 95% (2σ), over 40 tests. Natural frequencies with low signal-to-noise ratios are marked with *.

Natural	Healthy	Elements damaged [Hz]				Variation	Damaged
frequency No.	[Hz]	26	41	66	69	2σ [Hz]	detectible?
1	3.2	1.7	1.8	2.1	2.2	0.4	Yes
2	4.0	2.5	2.5	2.6	2.4	0.1	Yes
3*	7.0	5.2	6.8	6.3	6.8	1.3	No
4*	9.3	8.9	8.7	8.5	8.6	0.3	Yes
5*	13.0	10.9	10.7	9.9	10.4	0.8	Yes
6*	15.3	14.2	13.2	13.7	14.3	0.9	Yes
7*	17.3	16.7	14.7	15.3	16.0	1.5	No

contain more uncertainty and thus a variation limit of 2σ is acceptable since it is well above sensor resolution.

5.1. Damage detection

5.1.1. Frequency analysis of the half-tensegrity structure, prior to mid-span connection

Table 2 shows the average natural frequencies from ten tests of the half structure from the healthy state and the damaged state for ruptured Elements 26, 41, 66, and 69 using SOBI to separate natural frequencies. Changes in frequency between healthy and cable rupture events are greater than the variation limit of two standard deviations in units of Hertz and are therefore detectible. Detectible damage is noted as yes when natural frequencies from all ruptured cables are beyond the variation of 2σ, possible when some of the rupture cables are beyond the variation of 2σ, and no when none of the natural frequencies from the rupture cables are beyond the variation of 2σ. Tests with signal-to-noise (SNR) value of less than a factor of approximately 20 (Akande et al., 2016) in Table 2 are marked with a star.

The mean percent change between all healthy (column 2) and all damaged state tests (columns 3-6) is approximately 19%. However, the mean percent change per natural frequency from columns 3-6 of Table 2 is approximately 5%. Given a threshold of damage detection of 2σ, the mean variation is 0.8 [Hz] and damage is clearly detected in 5 of the 7 cases for the half-tensegrity structure. Although detection of a damaged element is possible,

determination of which cable is damaged presents a challenge since the differences in values after damage are below the threshold of noise.

5.1.2. Frequency analysis of the full-tensegrity structure, in-service condition

Free-vibration tests on the structure are successful at extracting only the first natural frequencies with low signal-to-noise ratios. Using a forcing frequency from a motor installed at mid-span of the structure, a stronger response results in a clearer identification of natural frequencies. The motor moved a cylindrical mass of 0.25 [kg] with an amplitude of 0.025 [m]. Setting the motor frequency to 5 [Hz], below the first natural frequency, results in high amplitude movement in healthy and damaged states. Knowing the forced frequency and oscillating mass, the frequency response function (FRF) is developed to determine the contribution of frequencies to the measurements.

Figure 7 shows the fast Fourier transform (FFT) of the response of one sensor during one test of free-vibration and frequency response due to forced-vibrations of ruptured Element 26. Units of the vertical axis are of the original nodal position input, [cm], divided by the discretization in the frequency domain of the FFT (signal length of approximately 30 [s] at 165 [Hz]). Despite there being more natural frequencies observed by other sensors, only the first two natural frequencies, 5.8 [Hz] and 10.8 [Hz], are visible in the sample response. Although the first natural frequency is visible for both vibration tests, the first natural frequency response is only statistically significant for the frequency response due to forced-vibration. The improved signal following the FRF due to forced-vibrations is useful for determining natural frequencies of the full-tensegrity structure.

Table 3 shows the natural frequencies of the full structure from the healthy and damaged states using forced-vibration measurements for ten rupture tests of Elements 26, 41, 66 and 69. Variation is two standard deviations in units of Hertz. Changes in frequency between healthy and cable rupture events are greater than the variation limit and are therefore detectible.

The mean percent change between all healthy (column 2) and all damaged state tests (columns 3-6) is approximately 12%. However, the mean percent change per natural fre-

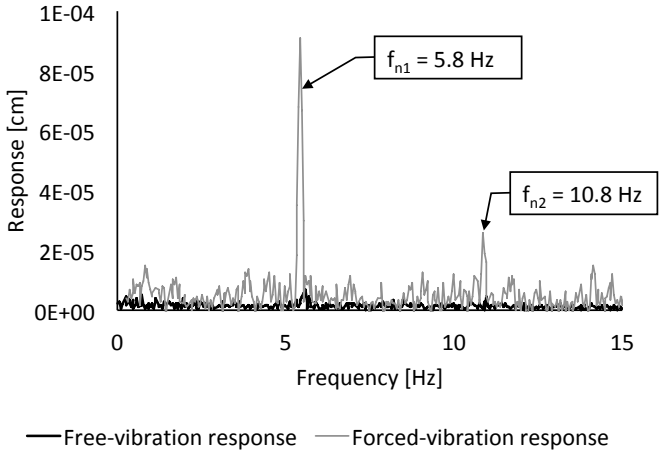

Figure 7: Sample free-vibration and forced-vibration structural response following the rupture of Element 26.

Table 3: Average measurements of natural frequencies from the full structure for ten forced-vibration rupture tests of Elements 26, 41, 66, and 69 including variation of 2 standard deviations, approximately 95%, over 40 tests. Natural frequencies with low signal-to-noise ratio are marked with a star.

Natural frequency No.	Healthy [Hz]	Elements damaged [Hz] 26	41	66	69	Variation 2σ [Hz]	Damaged detectible?
1	5.8	5.5	5.6	4.7	4.9	0.7	Possible
2	10.8	8.5	9.2	8.1	9.1	0.9	Yes
3	16.9	15.4	13.9	14.4	15.5	1.3	Yes
4*	21.2	19.7	16.3	19.8	17.7	2.9	Possible
5*	24.8	23.0	23.0	24.1	24.1	1.1	Possible
6*	29.6	26.3	27.5	26.1	26.7	1.1	Yes

quency from columns 3-6 of Table 3 is approximately 5%. Damage detection between healthy and damaged states is therefore possible since the percent change is greater than typical noise levels of 5%. Given a threshold of damage detection of 2σ, the mean variation is 1.3 [Hz] and damage is detected in up to 5 of the 6 cases for the full-tensegrity structure. Damage location (determination of which cable) using natural frequencies is not possible, as observed for the half-structure.

5.2. Damage location

Figure 8 shows the procedure of implementing error-domain model falsification (EDMF) (see Section 2.2) with moving window principal component analysis (MWPCA) (see Section 2.3). Model, and measurements of the healthy and damaged structure, as well as parameters of uncertainty and measurement error are required for damage location. This procedure follows a positive result for damage detection from the previous section. Limits and sensitivity of the model to each parameter are determined using Latin Hypercube Sampling (LHS) (McKay et al., 1979). This method determines combined uncertainties for the Monte-Carlo analysis (Goulet et al., 2013) associated with nodal positions during a cable rupture event. Once all parameters are tested (see Table 4), primary and secondary parameters are grouped and form model classes based on the sensitivity to model response. Using these model classes, candidate scenarios are generated by varying parameter values.

5.2.1. Position-based error-domain model falsification (EDMF)

The principle of EDMF is to determine which candidate scenarios of damage location lie within the uncertainty thresholds (see Figure 1) by calculating differences between model prediction and measurement. A possible scenario becomes a candidate scenario only if all differences are within the threshold limits at all measurement locations. The target reliability of identification is fixed at 95%. Nodal positions are instrumented with sensors are used to compare measurement and simulation. Changes in position measured at nodes due to a ruptured cable that are equally reflected in a candidate scenario suggest that the simulation is in the region of rupture location.

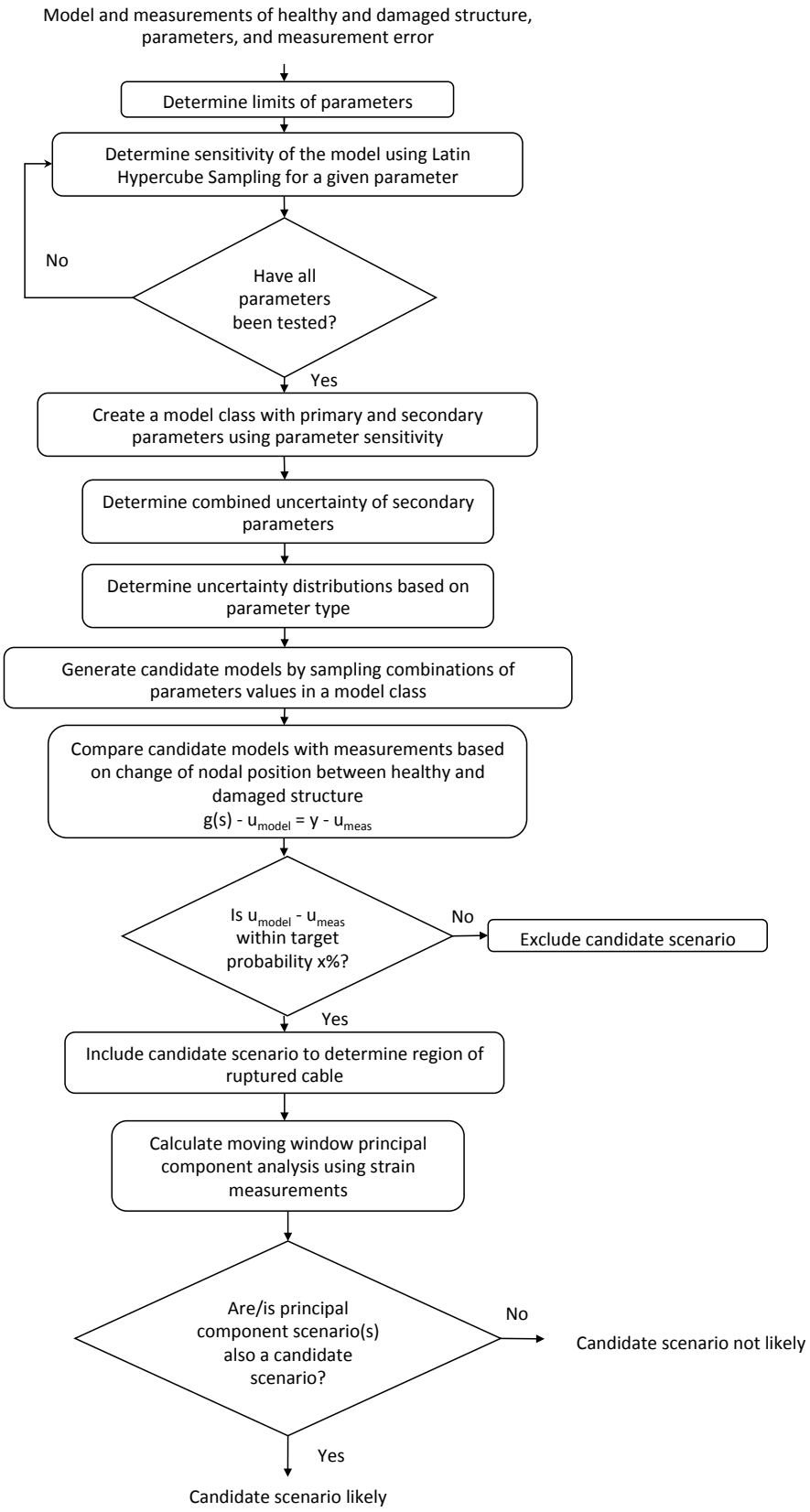

Figure 8: Procedure of implementing error-domain model falsification (EDMF) with moving window principal component analysis (MWPCA) for damage location. See Section **??** for terminology.

Table 4: Parameter value ranges and sensitivity to parameter variation for exclusion of a possible scenario

Parameter	Variable	Lower bound	Mean	Upper bound	Sensitivity to model response	
					Half (%)	Full (%)
Joint eccentricity	e [mm]	0	15	30	47	26
Young's modulus	E [GPa]	66.5	70	73.5	11	21
Coefficient of friction	μ	0.1	0.15	0.4	20	25
Support stiffness (equivalent)	k [N/m]	80%	100%	100%	8	5
Cable tension factor	F	0.9	1.0	1.1	14	23

Lastly, moving window principal component analysis (MWPCA) is applied to strain measurements on elements and compared with the region of rupture location. The change in eigenvalues between measurements of the healthy and damage structure is calculated. Elements of the structure that are influenced by cable rupture the most are the most sensitive participating components in the eigenvalues. Since the rupture of a cable itself cannot participate in MWPCA, rupture of the cable affects nearby cables.

5.2.2. Parameters for damage location

Locations of the ruptured cable in damage scenarios are excluded through comparing measured and predicted nodal positions after the rupture event. The parameters identified for generation of scenarios include: eccentricity of the joints, Young's modulus of elasticity, coefficient of friction at nodes for sliding cables, stiffness of the supports, and tension variation in cables. Table 4 shows the upper and lower bounds of each parameter.

Sources of uncertainty, including measurement error and modeling error, are included with values assigned by engineering judgement. Modeling error and measurement error are assigned a uniform distribution with boundaries of 6 - 9% and 1 - 3% respectively for the half structure and 5 - 22% and 2 - 14% respectively for the full structure. These boundary values are obtained by a parameter sensitivity analysis of model response.

The sensitivity analysis is the linear regression of each variable on the Monte-Carlo sampling-generated analysis. The importance of each parameter is determined; the two

largest contributors to variation of model response were joint eccentricity and coefficient of friction. The remaining parameters of Table 4 are classified as secondary parameters that contribute to the definition of threshold levels through combination of uncertainties, see Section 2.2.

5.2.3. Strain-based moving window principal component analysis (MWPCA)

Strain values have been measured at four cable elements and three strut elements (see Figure 3). Strain gauges were not installed on every elements since monitoring of every element would not be possible for civil engineering structures. Sets of measurements consist of the difference in strain, are averaged over 10 seconds, of nodes prior and post rupture event. Strain measurements from the tensegrity structure do not have a sufficient signal-to-noise ratio for modal extraction.

Principal component analysis (PCA) is used for dimensionality reduction of measurements for damage location through eliminating eigenvalues having changes below a threshold of 6σ. Despite measurements with a low signal-to-noise ratio such as those from the strain gauges, this method successfully locates changes in properties of the structure. Eigenvectors from the significant principal components are related to sensors. Using a moving window PCA (MWPCA) as proposed by Posenato et al. (2008), eigenvectors have been monitored for changes greater than 6σ before, during, and after damage events.

The window size of the MWPCA has been set such that the rank of matrix produced by the eigenvectors of the window is a maximum value of three. For a recording frequency (F_s) of 165 [Hz], significant changes in eigenvectors are consistent in simulations with window lengths up to $0.4F_s$ without compromising data resolution. Varying percentage values of overlapping windows is tested using strain measurements. Although a small amount of overlap, such as 10%, provided clearer principal components, there is not a clear benefit to a higher degree of overlap, such as 60%, for damage detection using strain measurements of the deployable tensegrity structure.

5.2.4. Damage location for the half-tensegrity structure

Figure 9 shows differences between model and measurements for measurement events of four cable ruptures. The total number of scenarios is shown as black outlined bars, candidate scenarios are shown as filled bars and 95% thresholds shown with a dashed line. Considering all measurement locations and measurement events for the half-tensegrity structure, an average of 70% candidate scenarios are excluded. The candidate scenario that have the correct location of the ruptured element is not excluded. When no cable was damaged, all possible scenarios are excluded. Cable elements surrounding the true ruptured cable and several at the free end of the structure also are not excluded. Despite the half structure having fewer cable elements than the full structure, low stiffness of the half-tensegrity structure complicates location of damaged elements.

Figure 10 shows candidate scenarios in terms of position from the east support for damage of Elements 26, 41, 66, and 69 on the half-tensegrity structure (see Figure 4 for reference position). Standard deviation of 2σ over ten repetitions are shown for each interval by black range indicators.

Locations of elements on the structure having statistically significant (6σ) changes in eigenvectors taken from equally significant principal components for strain measurements are shown as vertical dashed grey lines. As mentioned earlier, the number of standard deviations for eigenvectors is higher than for natural frequency extraction (2σ) due to possible resolution in the time domain versus the frequency domain restricted by sampling frequency of measurements. The location of the element (true location) is indicated by a black dot. Damage location using EDMF is successful in all four cases. Using MWPCA on strain measurements in adjacent elements is not as successful. However, at least one of the elements identified by MWPCA is close to the true damage location.

5.2.5. Damage location for the full-tensegrity structure

Once the two halves are connected, the elements are more coupled than in the half structure and thus, the amount of nodal-position change is reduced. Figure 11 shows differences between model and measurement positions for measurement events for a cable rupture for

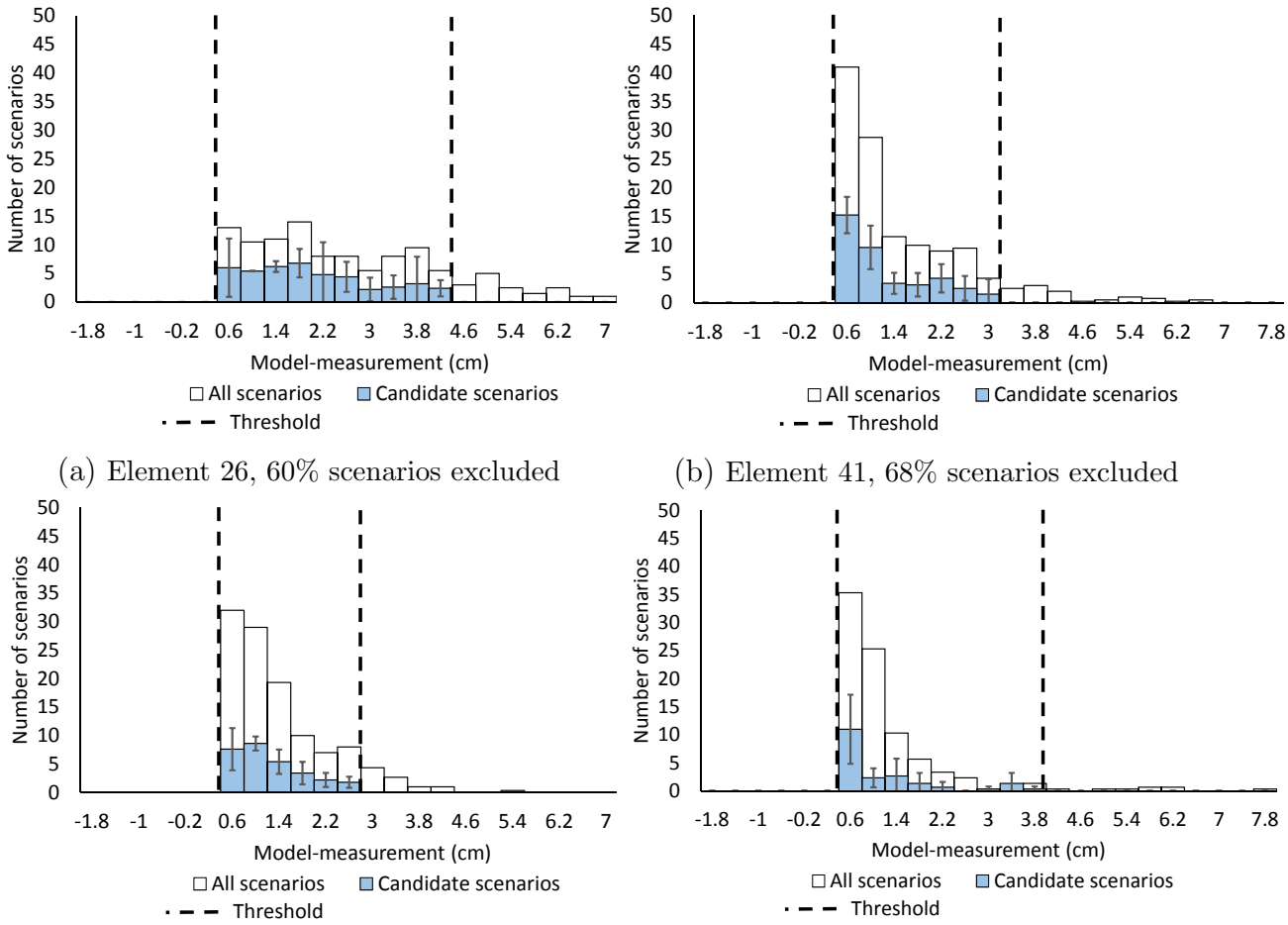

(a) Element 26, 60% scenarios excluded

(b) Element 41, 68% scenarios excluded

(c) Element 66, 70% scenarios excluded

(d) Element 69, 77% scenarios excluded

Figure 9: Number of scenarios versus the difference between model and measured change in position of the half-tensegrity structure. The total number of scenarios is shown as the black outlined bars and the candidate scenarios are shown as the filled bars as well as the 95% thresholds shown with a dashed line. All candidate scenarios are within the thresholds.

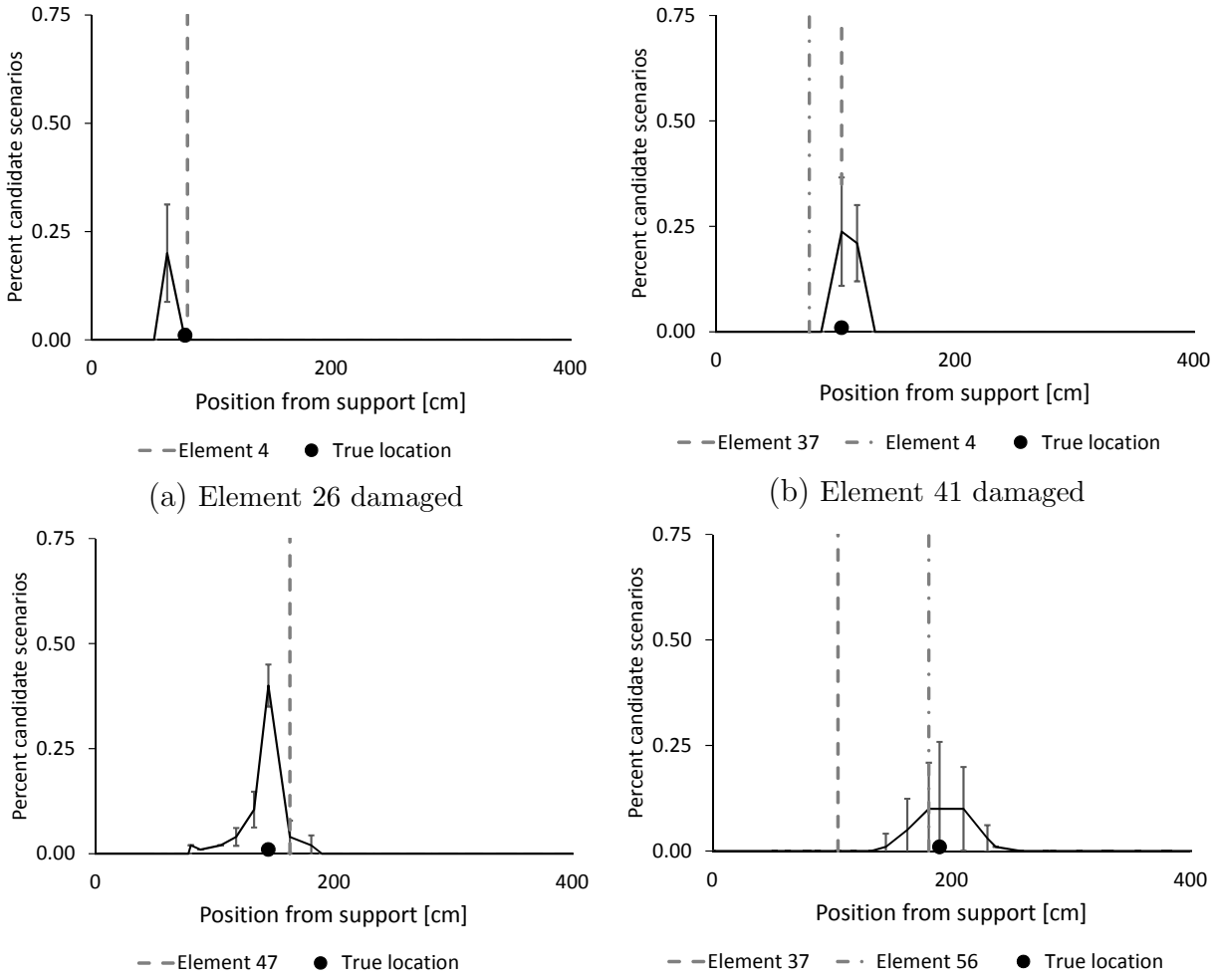

(a) Element 26 damaged

(b) Element 41 damaged

(c) Element 66 damaged

(d) Element 69 damaged

Figure 10: Percent of candidate scenarios using position measurements relative to position from the support on the half-tensegrity structure. Standard deviation of 2σ over ten repetitions are shown for each interval by black range indicators. Locations of elements on the structure having statistically significant (6σ) changes in eigenvectors taken from equally significant principal components for strain measurements are shown as vertical dashed grey lines.

the full structure. The total number of scenarios is shown as black outlined bars, candidate scenarios are shown as filled bars, and 95% thresholds shown with a dashed line. Considering all measurement locations and measurement events for the full-tensegrity structure, an average of 71% possible scenarios are excluded. When no cable is damaged, all possible scenarios are excluded.

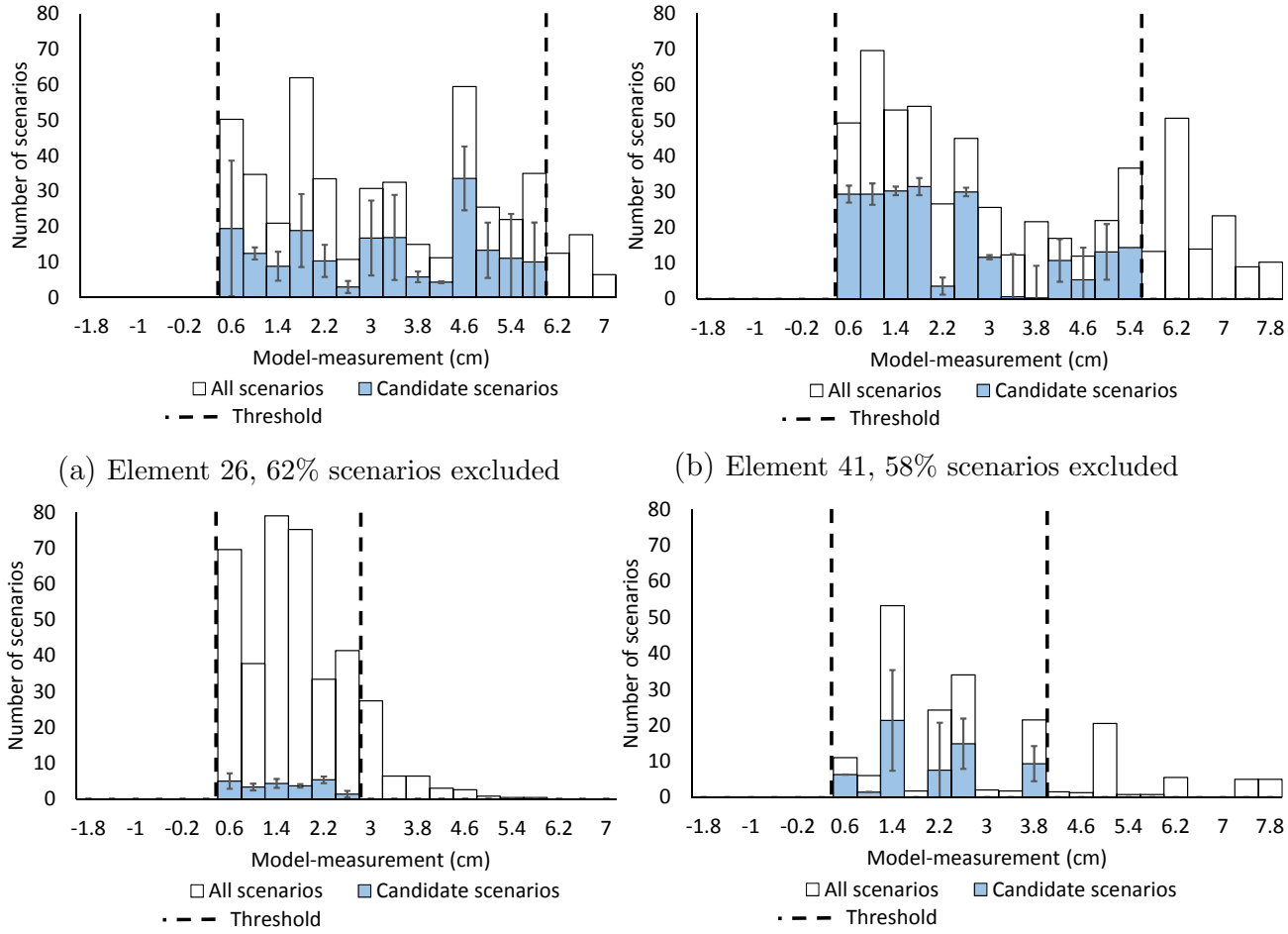

(a) Element 26, 62% scenarios excluded

(b) Element 41, 58% scenarios excluded

(c) Element 66, 94% scenarios excluded

(d) Element 69, 69% scenarios excluded

Figure 11: Histogram of number of scenarios for differences between model and measured change in position of the full-tensegrity structure. The total number of scenarios is shown as black outlined bars, candidate scenarios are shown as filled bars, and 95% thresholds shown with a dashed line. All candidate scenarios are within the thresholds.

Figure 12 shows candidate scenarios in terms of position from the east support for damage of Elements 26, 41, 66, and 69 on the full-tensegrity structure (see Figure 4 for reference

position). Standard deviations of 2σ over ten repetitions are shown for each interval by black range indicators. EDMF successfully identifies the position of the true damaged element in all four cases.

6. Discussion

Table 5 describes the advantages and challenges of the methods presented for damage detection and location: frequency analysis, EDMF using node position measurements, and MWPCA using strain measurements. Methods are implemented separately without combination. Using natural frequencies, damage are detected in 5 of the 7 cases for the half-tensegrity structure and 5 of the 6 cases for the full-tensegrity structure. Damage location is not possible using natural frequencies of the structure. The modal assurance criterion (MAC) is a statistical indicator used to detect large changes in mode shapes (Allemang, 2003) and has not been applied since structural mode shapes from the topology of this tensegrity structure are not useful because their complexity does not support damage detection and location.

The first advantage of model-based damage detection (EDMF) over MWPCA is that measurement sets pre- and post- damage are treated as discrete events. Applying error-domain model falsification to nodal position measurements, the probable region of damage is successfully detected and located. However, instrumentation using position tracking to submillimeter resolution is costly and results are sensitive to the amount of uncertainty that is present.

The advantages of applying MWPCA to strain measurements are that instrumentation is inexpensive and that changes in eigenvectors are easily detected despite input with a high degree of noise. Using MWPCA, elements adjacent to the true location of the damaged element may be found. However, weak signals do not successfully detect eigenvector values greater than 6σ and detection is only possible for the specific elements measured. It is expected that these detection and location strategies will be successful for a range of cable-strut structures under similar conditions.

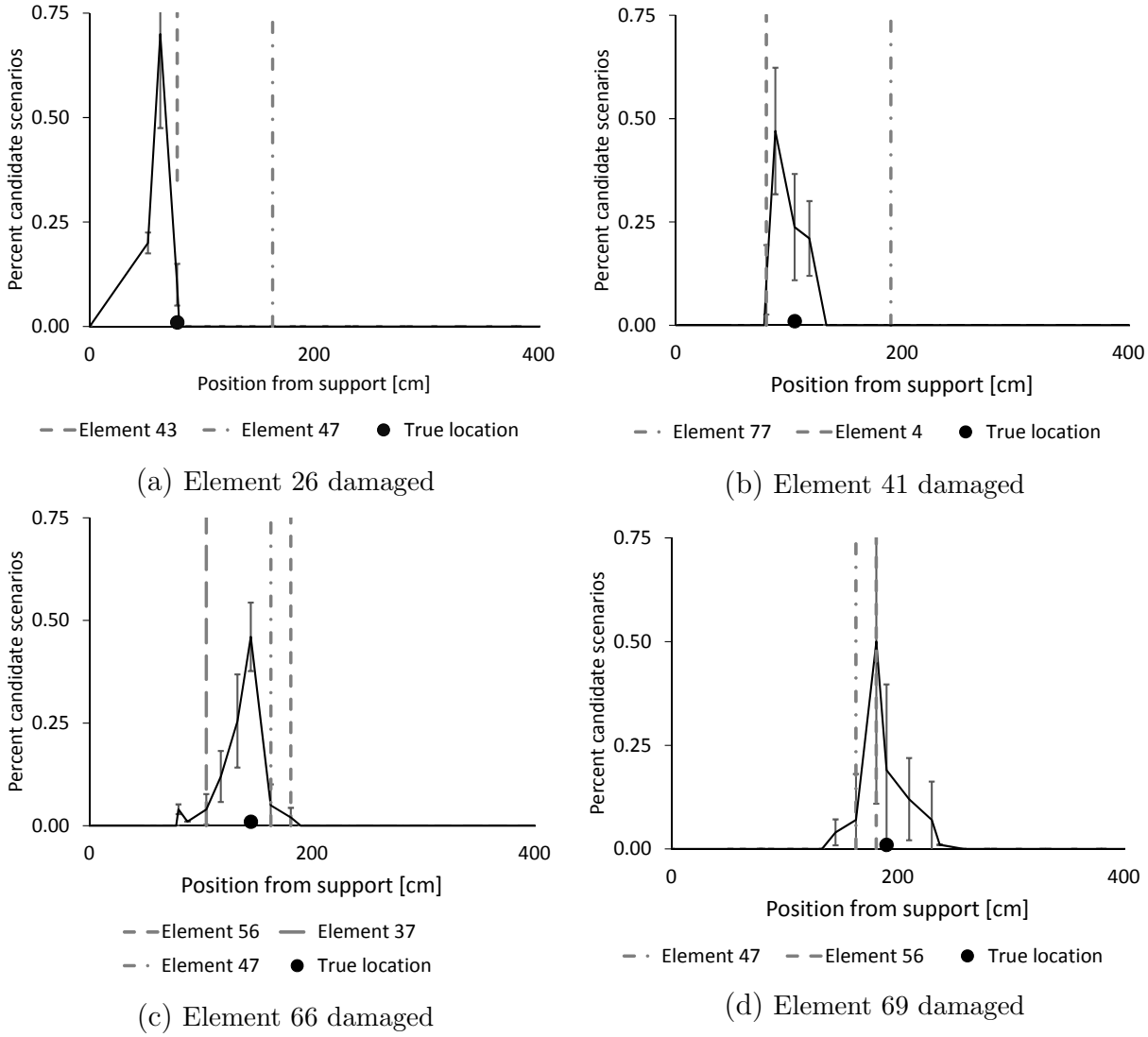

(a) Element 26 damaged

(b) Element 41 damaged

(c) Element 66 damaged

(d) Element 69 damaged

Figure 12: Percent of candidate scenarios using position measurements relative to position from the support on the full-tensegrity structure. Standard deviation of 2σ over ten repetitions is shown for each interval by black range indicators. Locations of elements on the structure having statistically significant (6σ) changes in eigenvectors taken from equally significant principal components for strain measurements are shown as vertical dashed grey lines.

Table 5: Advantages (+) and challenges (-) of three methods have been described for detection and location of ruptured cables of the full and half-tensegrity structure.

	Detection	Location
Frequency analysis using SOBI	+ Easy on-site measurement	—
	- Damage not detected in all frequencies	—
EDMF	+ Detection of probable region possible	+ Location of probable region
	- Expensive instrumentation (position tracking)	- Results may be sensitive to the level of uncertainty
MWPCA	+ Inexpensive instrumentation (strain gauges)	+ May find elements that are adjacent to the rupture
	- No information when low signal-to-noise ratio	- Adjacent elements need to be instrumented. Not reliable.

7. Conclusions

Detection of a broken element is successful by observing differences of natural frequencies between healthy and damaged states. Natural frequencies are easily identified for the half-tensegrity structure comparing measured ambient vibrations and simulation. For the full-tensegrity structure, using forced-vibrations such that source separation using second-order blind identification (SOBI) is possible.

Location of a ruptured cable is successful using nodal position measurements through excluding damage scenarios and using strain measurements to identify elements of significant changes in eigenvector coefficients using principal component analysis. Implementing error-domain model falsification to exclude possible scenarios for location of damaged elements successfully reduced the number of probable cases. An average of 70% of possible scenarios for the half structure and 71% for the full structure are excluded in the process of location. Elements with strain sensors in proximity to true ruptured elements are successfully identified as the most affected by rupture events, thus indicating the location of a ruptured cable. Therefore, the methodology involving error-domain model falsification (EDMF) for damage location is useful for closely-coupled structures that are capable of large shape changes.

At least one of the elements identified by moving window principal component analysis (MWPCA) successfully indicated damage in an element in the region of the true location of rupture. It is expected that this method for damage location will be successful for a range of cable-strut structures under similar conditions.

The original contribution of this paper is an evaluation of the ability of several methods to detect and locate damage in a near-full-scale deployable tensegrity structure. All methods implemented can be applied to other active structures. These methods thus reveal the potential for self-diagnosis of complex sensed structures.

Acknowledgements

The research is sponsored by funding from the Swiss National Science Foundation under project number 200020_169026.

References

Adam, B., Smith, I. F. C., 2007a. Self-diagnosis and self-repair of an active tensegrity structure. Journal of Structural Engineering 133 (12), 1752–1761.

Adam, B., Smith, I. F. C., 2007b. Tensegrity active control: Multiobjective approach. Journal of Computing in Civil Engineering 21 (1), 3–10.

Akande, K., Iqbal, N., Zerguine, A., Chambers, J., 2016. Normalised frequency-domain soft constraint satisfaction multimodulus blind algorithm. Electronics Letters 52 (3), 239–241.

Akgün, Y., Gantes, C. J., Sobek, W., Korkmaz, K., Kalochairetis, K., 2011. A novel adaptive spatial scissor-hinge structural mechanism for convertible roofs. Engineering Structures 33 (4), 1365–1376.

Allemang, R., 2003. The modal assurance criterion - twenty years of use and abuse. Sound and Vibration 37 (8), 14–21.

Ashwear, N., Eriksson, A., 07 2014. Natural frequencies describe the pre-stress in tensegrity structures. Computers & Structures 138 (02), 162–171.

Ashwear, N., Eriksson, A., 2017. Vibration health monitoring for tensegrity structures. Mechanical Systems and Signal Processing 85, 625–637.

Beck, M. B., 1987. Water quality modeling: A review of the analysis of uncertainty. Water Resources Research 23 (8), 1393–1442.

Bel Hadj Ali, N., Rhode-Barbarigos, L., Pascual Albi, A., Smith, I. F. C., 2010. Design optimization and dynamic analysis of a tensegrity-based footbridge. Engineering Structures 32 (11), 3650–3659.

Bel Hadj Ali, N., Rhode-Barbarigos, L., Smith, I. F. C., 2011. Analysis of clustered tensegrity structures using a modified dynamic relaxation algorithm. International Journal of Solids and Structures 48 (5), 637–647.

Belouchrani, A., Abed-meraim, K., 1997. Using Second-Order Statistics. IEEE Transactions on Signal Processing 45 (2), 434–444.

Beven, K., Binley, A., 1992. The future of distributed models: Model calibration and uncertainty prediction. Hydrological Processes 6 (3), 279–298.

Beven, K. J., Smith, P. J., Freer, J. E., 2008. So just why would a modeller choose to be incoherent? Journal of Hydrology 354 (1-4), 15–32.

Bhalla, S., Panigrahi, R., Gupta, A., 2013. Damage assessment of tensegrity structures using piezo transducers. Meccanica 48 (6), 1465–1478.

Blasone, R. S., Vrugt, J. A., Madsen, H., Rosbjerg, D., Robinson, B. A., Zyvoloski, G. A., 2008. Generalized likelihood uncertainty estimation (GLUE) using adaptive Markov Chain Monte Carlo sampling. Advances in Water Resources 31 (4), 630–648.

Day, A. S., 1965. An introduction to dynamic relaxation (dynamic relaxation method for structural analysis, using computer to calculate internal forces following development from initially unloaded state). The Engineer 219, 218–221.

Doebling, S., Farrar, C. R., Prime, M., Shevitz, D., 1996. Damage identification and health monitoring of structural and mechanical systems from changes in their vibration characteristics: A literature review. Tech. rep., Los Alamos National Laboratory.

Dubé, J. F., Angellier, N., Crosnier, B., jul 2008. Comparison between experimental tests and numerical simulations carried out on a tensegrity minigrid. Engineering Structures 30 (7), 1905–1912.

Fan, W., Qiao, P., 2010. Vibration-based Damage Identification Methods: A Review and Comparative Study. Structural Health Monitoring 10 (1), 83–111.

Friswell, M. I., 02 2007. Damage identification using inverse methods. Philosophical transactions. Series A, Mathematical, physical, and engineering sciences 365, 393–410.

Gantes, C. J., Connor, J. J., Logcher, R. D., Rosenfeld, Y., 1989. Structural analysis and design of deployable structures. Computers and Structures 32 (3-4), 661–669.

Goulet, J.-A., Michel, C., Smith, I. F. C., 2013. Hybrid probabilities and error-domain structural identification using ambient vibration monitoring. Mechanical Systems and Signal Processing 37 (1-2), 199–212.

Kahla, N., Moussa, B., 2002. Effect of a cable rupture on tensegrity systems. International Journal of Space Structures 17 (1), 51–65.

Kahla, N. B., Kebiche, K., 2000. Nonlinear elastoplastic analysis of tensegrity systems. Engineering Structures 23 (09), 1552–1566.

Kebiche, K., Kazi-Aoual, M., Motro, R., 1999. Geometrical non-linear analysis of tensegrity systems. Engineering Structures 21 (9), 864–876.

Khellaf, N., Kebiche, K., 2013. Nonlinear analysis of hexagon-based tensegrity ring: Effect of slackened and yielded cables. KSCE Journal of Civil Engineering 17 (6), 1371–1382.

Laory, I., Trinh, T. N., Posenato, D., Smith, I. F., 2013. Combined Model-Free Data-Interpretation Methodologies for Damage Detection during Continuous Monitoring of Structures. Journal of Computing in Civil Engineering 27 (6), 657–666.

McKay, M. D., Beckman, R. J., Conover, W. J., 1979. A comparison of three methods for selecting values of input variables in the analysis of output from a computer code. Technometrics 21 (2), 239–245.

Motro, R., 2011. Structural morphology of tensegrity systems. Meccanica 46 (1), 27–40.

Motro, R., Maurin, B., Silvestri, C., 2006. Tensegrity rings and the hollow rope. In: IASS symposium Beijing, China.

Otter, J., 1965. Computations for prestressed concrete reactor pressure vessels using dynamic relaxation. Nuclear Structural Engineering 1 (1), 61–75.

Overschee, P. V., Moor, B. D., 1996. Continuous-time frequency domain subspace system identification. Signal Processing 52 (4), 179–194.

Pearson, K., 1901. On lines and planes of closest fit to systems of points in space. The London, Edinburgh, and Dublin Philosophical Magazine and Journal of Science 2 (1), 559–572.

Pellegrino, S., 2001. Deployable Structures. Spring-Verlag Wien, Vienna.

Pellegrino, S., Calladine, C., 1986. Matrix analysis of statically and kinematically indeterminate frameworks. International Journal Solids Structures 22 (4), 409–428.

Poncelet, F., Bernay, B., Kerschen, G., Golinval, J.-C., 2010. Damping material characterization and modeling : An industrial case-study. In: Proceedings of the ASME International Design Engineering Technical Conferences and Computers and Information in Engineering Conference 2009. Vol. 1. San Diego, California, pp. 881–888.

Popper, E. R., 1959. The Logic of Scientific Discovery. Vol. 12.

Posenato, D., Lanata, F., Inaudi, D., Smith, I. F. C., 2008. Model-free data interpretation for continuous monitoring of complex structures. Advanced engineering informatics 22, 135–144.

Rhode-Barbarigos, L., Jain, H., Kripakaran, P., Smith, I. F. C., 2010. Design of tensegrity structures using parametric analysis and stochastic search. Engineering with Computers 26 (2), 193–203.

Rhode-Barbarigos, L., Schulin, C., Ali, N., Motro, R., Smith, I. F. C., 2012. Mechanism-based approach for the deployment of a tensegrity-ring module. Journal of Structural Engineering 138 (4), 539–548.

Shekastehband, B., Abedi, K., 2014. Dynamic propagation of snap-through buckling in tensegrity structures. International Journal of Structural Stability and Dynamics 14 (01), 1350049.

Shekastehband, B., Abedi, K., Chenaghlou, M., 09 2011. Sensitivity analysis of tensegrity systems due to member loss. Journal of Constructional Steel Research 67 (9), 1325–1340.

Sidak, Z., 1967. Rectangular confidence regions for the means of multivariate normal distributions. Journal of the American Statistical Association 62 (318), 626–633.

Skelton, R. E., Adhikari, R., Pinaud, J.-P., Chan, W. L., 2001. An introduction to the mechanics of tensegrity structures. In: Conference on Decision and Control. Orlando, Florida, USA, pp. 4254–4259.

Smith, I. F. C., 2016. Studies of sensor data interpretation for asset management of the built environment. Frontiers in Built Environment 2, 8.

Snelson, K., 2012. The art of tensegrity. International Journal of Space Structures 27 (2-3), 71–80.

SOFiSTiK, 2017. SOFiSTiK. http://www.sofistik.com/.

Sultan, C., Corless, M., Skelton, R. E., jun 2002. Linear dynamics of tensegrity structures. Engineering Structures 24 (6), 671–685.

Sun, N., Hong, B., Hall, M., 2014. Assessment of the SWMM model uncertainties within the generalized likelihood uncertainty estimation (GLUE) framework for a high-resolution urban sewershed. Hydrological Processes 28 (6), 3018–3034.

Sychterz, A. C., Smith, I. F. C., 2017. Joint Friction during Deployment of a Near-Full-Scale Tensegrity Footbridge. Journal of Structural Engineering 143 (9), 1–10.

Tarantola, A., 2006. Popper, Bayes and the inverse problem. Nature physics 2 (8), 492–494.

Veuve, N., 2015. Towards biomimetic behavior of an active deployable tensegrity structure. Ph.D. thesis, Ecole polytechnique fédérale de Lausanne.

Veuve, N., Safaei, S. D., Smith, I. F. C., 2015. Deployment of a Tensegrity Footbridge. Journal of Structural Engineering 141 (11), 1–8.

Yin, T., Jiang, Q.-H., Yuen, K.-V., 2017. Vibration-based damage detection for structural connections using incomplete modal data by Bayesian approach and model reduction technique. Engineering Structures 132, 260–277.

Zhang, W., Li, T., 2015. The Influence of Objective Function and Acceptability Threshold on Uncertainty Assessment of an Urban Drainage Hydraulic Model with Generalized Likelihood Uncertainty Estimation Methodology. Water Resources Management 29 (6), 2059–2072.